Supporting Information

Co-fibrillization of pathogenic and functional amyloid proteins with gold nanoparticles against amyloidogenesis

Ibrahim Javed,[†] Yunxiang Sun,[§,#] Jozef Adamcik,[‡,#] Bo Wang,[§] Aleksandr Kakinen,[†] Emily H. Pilkington,[†] Feng Ding,[§] Raffaele Mezzenga,[‡] Thomas P. Davis,*[†,¶] and Pu Chun Ke*[†]*

[†]ARC Centre of Excellence in Convergent Bio-Nano Science and Technology, Monash Institute of Pharmaceutical Sciences, Monash University, 381 Royal Parade, Parkville, VIC 3052, Australia

[§]Department of Physics and Astronomy, Clemson University, Clemson, SC 29634, USA

[‡]Food & Soft Materials, Department of Health Science & Technology, ETH Zurich, Schmelzbergstrasse 9, LFO, E23, 8092, Zurich, Switzerland

[¶]Department of Chemistry, University of Warwick, Gibbet Hill, Coventry, CV4 7AL, United Kingdom

Discrete molecular dynamics simulations

Discrete molecular dynamics is a unique type of molecular dynamics algorithm with significantly enhanced sampling efficiency[1], which has been extensively used model nanoparticle-biomolecules interactions.[2, 3, 4] Detailed descriptions of the DMD method can be found elsewhere.[1, 5] We applied a united atom representation - i.e., explicitly modelling all polar hydrogen and heavy atoms - to model the proteins and fibrils. The interatomic interactions included *van der Waals*, solvation, electrostatic interactions and H-bonding. The solvation energy was estimated with the Lazaridis-Karplus implicit solvent model, EEF1.[6] The distance- and angular-dependent hydrogen bond interactions were modelled using a reaction-like algorithm.[7] Screened electrostatic interactions were modelled by the Debye-Hückel approximation.[8] A Debye length of 1 nm was used by assuming a water dielectric constant of

80 and a monovalent electrolyte concentration of 0.1 M. The Anderson's thermostat was used for the constant-temperature simulations.

Choice of amyloid-forming sequences in bLg

Mass-spectroscopy experiments showed that bLg amyloid fibrils were formed by a range of short peptide segments, which correlated with their hydrophobicity.[9] In this study, we chose the 6-residue segment ^{117}LACQCL^{122}, which has high hydrophobicity and corresponds to a short beta-strand in the native structure of bLg (Figure S2). Typically, a 6 or 7-residue sequence window has been used as a minimal length of amyloid peptides with amyloid-like aggregation behavior – e.g., GNNQQNY from yeast prion, sup35;[10] NFGAIL from IAPP;[11] and KLVFFAE from amyloid-β.[12] Additionally, it has also been shown in many cases sub-peptides corresponding to the amyloid core sequence of an amyloidogenic protein/peptide often share similar properties with the full-length protein/peptide, such as structure and cytotoxicity.[13, 14] Moreover, the LACQCL sequence contains two cysteines (three other cysteines are scattered in the full sequence or do not participate in the fibril[9] that are known to have strong affinity for Au, as confirmed by our binding simulations. Therefore, our choice of LACQCL captures the essential properties of AuNP coating with bLg and its subsequent co-fibrillization with IAPP.

Molecular systems in DMD simulations

We adopted the recently developed Au molecular mechanics force field[15] to model a spherical AuNP with a diameter of 40 Å that comprising 1,865 Au Atoms. The AuNP force field included both physical and chemical absorptions, aromatic and "image" charge interactions. The polarization was modelled by attaching a charged virtual particle (−0.3e) to each metal (0.3e) atom with a fixed bond length (1.0 Å) as implemented in the GolP force field.[15] Only the electrostatic interaction was taken into account for the virtual particle.

The known crystallography structure of native bLg was obtained from the RCSB Protein Data

Bank with the PDB code 3NPO.[16] The sequence of bLg amyloid-forming fragment LACQCL was picked based on previous mass spectrometry studies of bLg amyloids prepared at high temperature and low pH.[9, 17] Model bLg amyloids were subsequently built as double-layer β sheets with 10 peptides based on the zipperDB amyloid model of short peptides.[18] The double-layered IAPP protofibril model was generated based on the zipperDB energy landscape and the solid-state NMR constraints from the Tycko group,[19] which comprised 10 IAPP monomers. The basic and acidic residues of the IAPP (fibril) were assigned charges corresponding to their titration states at physiological condition (pH=7.4) – i.e., Arg and Lys residues were assigned +1e, Asp and Glu were assigned -1e, while His was neutral. Counter ions (Cl^-) were added to maintain the net charge of the systems zero and account for possible counter-ion condensation. All the fibril structures were energy minimized prior to the simulations.

Binding of single bLg amyloids with AuNP

The binding mechanism of each single protofibril with a 4 nm AuNP was probed. Specifically, five independent simulations with different initial inter-molecular orientations were carried out for each type of the protofibrils. As shown in Figure S2, the LACQCL protofibril could bind the AuNP with two different interfaces: having the fibril growth axis perpendicular to (mode 1; Figure S6d) and parallel to the AuNP surface (mode 2; Figure S2e). In mode 1, the LACQCL protofibril had one of the two fibril growth surfaces anchored on the AuNP surface. The mode 2 of the LACQCL protofibril had the beta-strand ends along the fibril surface contact the AuNP surface. In short, the protofibril formed by LACQCL could bind the surface of AuNP by more than one mode. For each type of the amyloid fibrils, we also computed the average binding energy of each binding mode as the energy difference between bound and unbound states (Figure S2).

Binding of heat-denatured bLg monomers with AuNP

To investigate the interaction between full-length and heat-denatured bLg and AuNP, DMD simulations of a bLg monomer and a 4 nm AuNP at ~350 K were performed. The bLg monomer was firstly placed 1.5 nm away from the AuNP (Figure S3c). As shown in Figure S3, the native structure of bLg mainly adopts β-sheets (~40%) and helices (~16%). Both β-sheet and helical structures were lost in less than 10 ns simulations at 350 K. However, the helical region (from D130 to K141) refolded when the bLg were bound on the AuNP surface (Figure S3f). Residues other than the helical region (D130 to K141) mainly assumed random coils and covered the AuNP surface (Figure S3c, f). The evolution of each residue's distance to the AuNP surface (Figure S3b, Cα atom of each residue was used in the calculation) revealed that most bLg residues bound the AuNP surface in less than 50 ns. This indicates that bLg monomers bound AuNPs at 350 K mostly in random coils, with residues D130-K141 retaining their native helical structure.

Binding of multiple bLg amyloids with AuNP

To investigate the self-assembly of multiple amyloids on the AuNP surface, we randomly placed 10 decameric protofibrils on the surface of an AuNP initially separated from each other. For each fibril type, we performed five independent DMD simulations. In all cases, the protofibrils could assemble by moving around the AuNP surface and by inter-amyloid interactions, leaving the open surface region of the AuNP available for additional amyloid fibrils to bind. As a result, amyloids are expected to fully cover the AuNP surface rendering a 'hard' amyloid-AuNP corona. Only the amyloids with binding mode 1 (Figure S2) had their fibril growth interface exposed and available for potential "seeding" of amyloid growth.

Docking between IAPP and bLg fibrils using DMD simulations

The model structures of the IAPP fibril derived from solid-state NMR[19] and the double-layer LACQCL fibril were used in the docking simulation. The β sheets from the two types of

amyloids were pre-aligned in parallel or anti-parallel by shifting each residue. For each initial alignment, 25 ns DMD simulations were performed for structural relaxation and binding energy estimation. The binding energy, ΔG, was estimated as the potential energy difference between the complex after equilibration and the unbound state (Figure 3). The lowest binding energy corresponded to a parallel binding between ^{8}ATQRLA^{13} and ^{26}ILSSTN^{31} of the IAPP and bLg fibril.

Table S1. IAPP fibrillation kinetic parameters in the presence of the two types of AuNPs.

Sample	Lag Time (min)	k (min^{-1})	$t_{1/2}$ (min)
IAPP control	168.3 ± 26.3	0.03 ± 0.001	230 ± 5
bLg AuNPs (0.083 mM)	232.1 ± 31.4	0.04 ± 0.009	285 ± 7
bLg AuNPs (0.11 mM)	181.4 ± 29.9	0.03 ± 0.005	240 ± 15
bLg-HDM AuNPs	113.6 ± 22.7	0.02 ± 0.001	225 ± 13

Table S2. Hydrodynamic sizes and zeta potentials of the two types of AuNPs.

AuNPs	Hydrodynamic Size (nm)	Zeta potential (mV)
bLg-AuNPs	24 ± 3	-15.8 ± 2.4
bLg-HDM AuNPs	20 ± 3	-21.6 ± 2.1

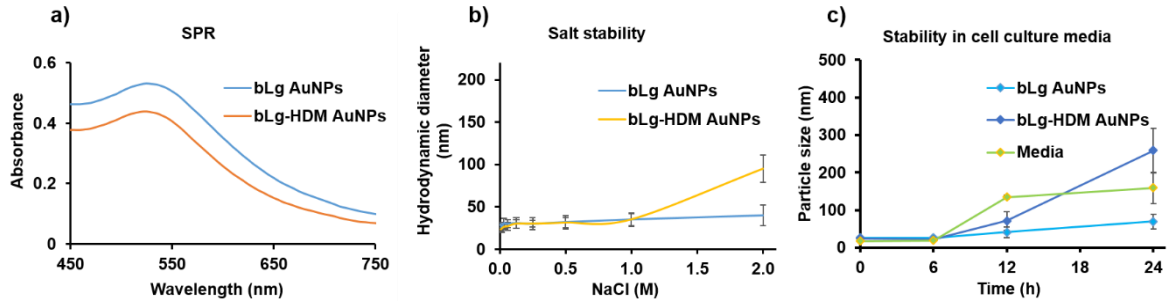

Figure S1. Characteristic surface plasmon resonance (SPR) peaks of the AuNPs at ~550 nm (a). Stability of the AuNPs against NaCl (b). AuNPs stability in cell culture media enriched with 15% fetal bovine serum (FBS) (c).

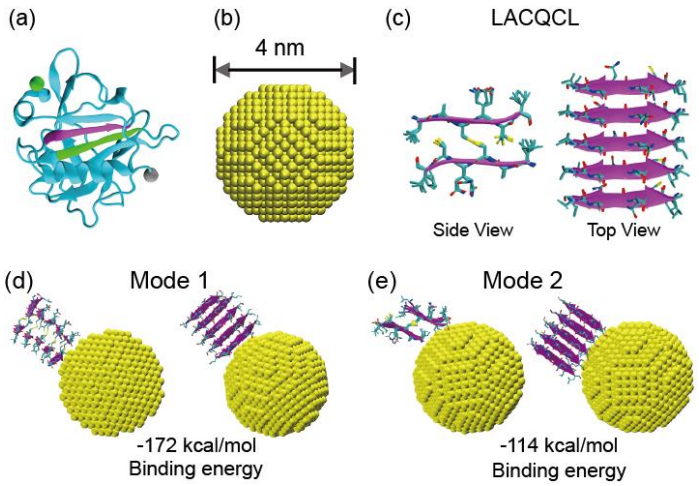

Figure S2. The molecular structures used in the DMD simulations. (a) The structure of the bLg (PDB ID: 3NPO) in cartoon representation with the Cα atoms in the N- and C-termini shown as grey and green beads, respectively. Two of the experimentally-identified amyloid-forming fragments, ^{112}LACQCL^{117} and ^{21}SLAMAAS^{27}, are colored in purple and green, respectively. (b) The structure of AuNP with a diameter of 4 nm is shown in sphere representation. (c) The model structure of decameric protofibrils formed by 10 LACQCL. The peptides are shown in two different views (Side and Top). The binding modes of the protofibril formed by LACQCL (d, e) on the AuNP surface are shown in two different views. The LACQCL protofibril can directly bind AuNP with two different interfaces: one has the fibril growth axis perpendicular to the AuNP surface (mode 1; d), and the other has the fibril growth axis parallel to the AuNP surface (mode 2; e).

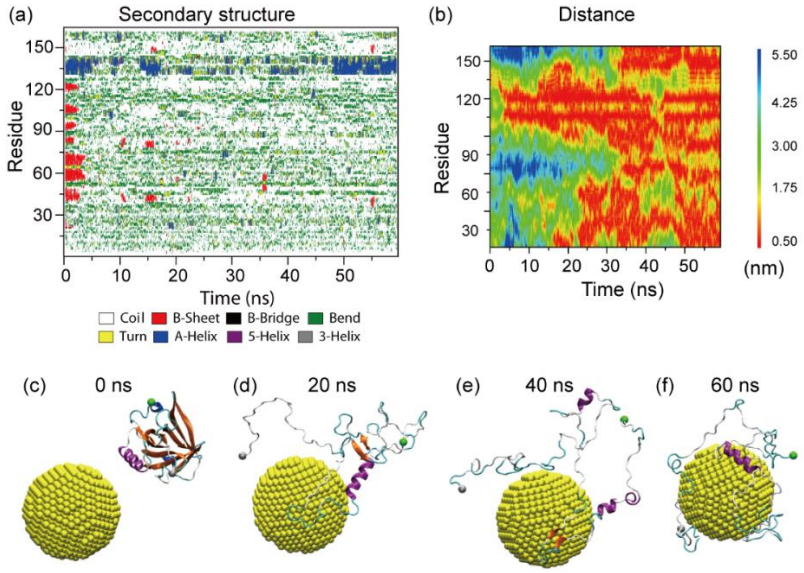

Figure S3. Coating of a bLg monomer on an AuNP at 350 K. (a) Time evolution of the secondary structure of each amino acid in full-length bLg (162 residues) at the surface of the 4 nm AuNP. (b) Time evolution of each residue's distance to the AuNP surface (Cα atom of each residue is used in calculation). (c-f) Snapshots along the simulation trajectory at 0, 20, 40 and 60 ns. The protein structures are shown as cartoons with α helices displayed in purple, β sheets in orange, turns in cyan, and coils in grey. The Cα atoms in the N- and C-termini are shown as grey and green beads, respectively.

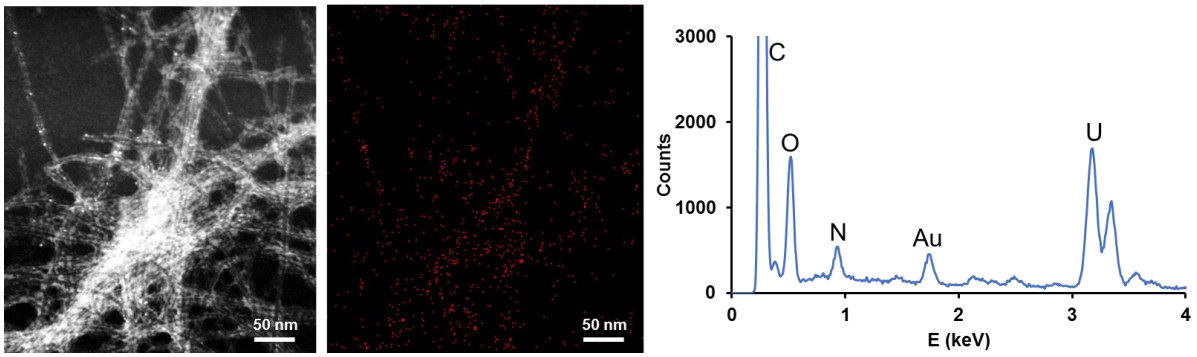

Figure S4. Energy-dispersive X-ray spectroscopic (EDX) mapping of bLg AuNPs in IAPP fibrils (middle), showing the peak of element Au (right) for the TEM image (HAADF mode) on the far left.

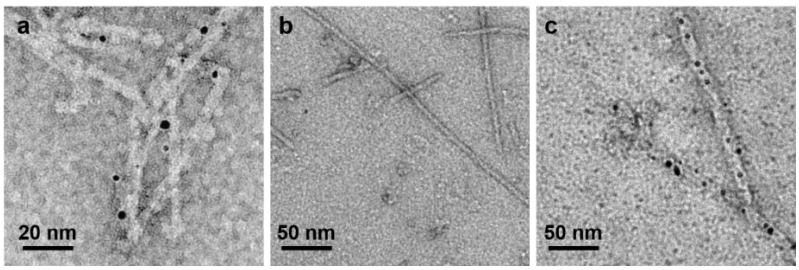

Figure S5. (a) bLg AuNPs (0.11 mM) adsorbed on IAPP fibril surfaces. Amyloid-β (1-42) incubated alone (b) and in the presence of bLg AuNPs (c). Incubation: 48 h.

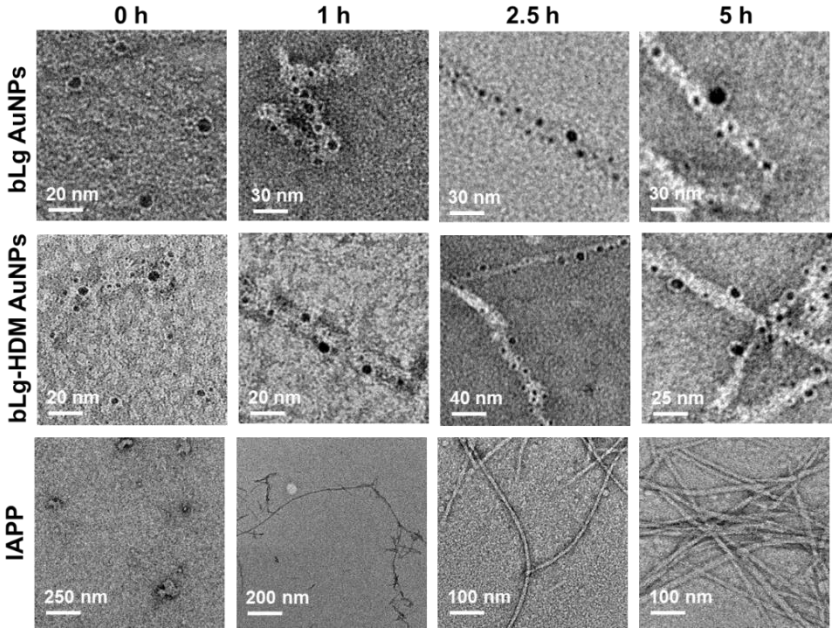

Figure S6. TEM imaging of the AuNPs incubated with IAPP. The interactions between the AuNPs and IAPP started to occur within the first hour, while intercalation of bLg AuNPs with IAPP appeared largely complete within 5 h.

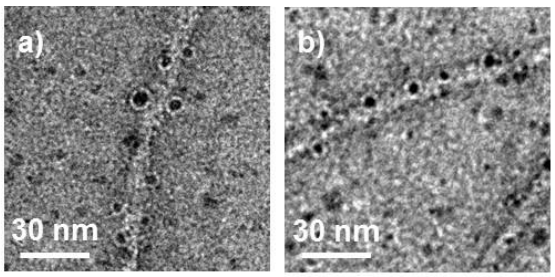

Figure S7. TEM imaging of bLg AuNPs (a) and bLg-HDM AuNPs (b) incubated for 4 h with preformed IAPP fibrils (2 day old).

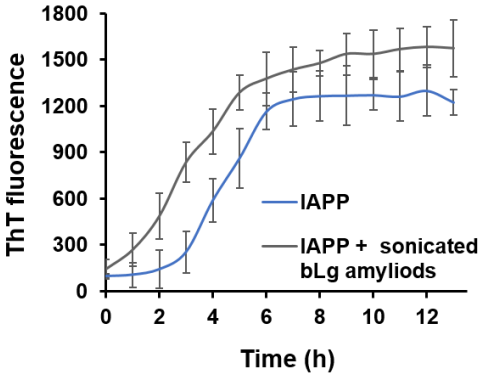

Figure S8. ThT assay of seeding IAPP monomers with sonicated bLg amyloids.

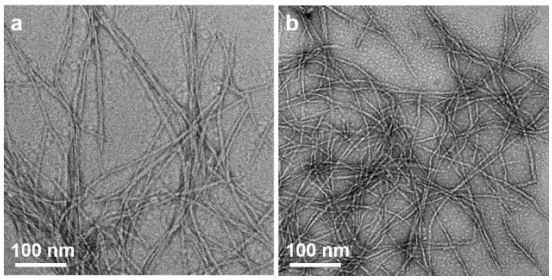

Figure S9. IAPP fibrils before (a) and after (b) X-ray irradiation.

References:

1. Ding, F.; Tsao, D.; Nie, H.; Dokholyan, N. V. *Structure* **2008**, 16, 1010-1018.
2. Radic, S.; Nedumpully-Govindan, P.; Chen, R.; Salonen, E.; Brown, J. M.; Ke, P. C.; Ding, F. *Nanoscale* **2014**, 6, 8340-8349.
3. Nedumpully-Govindan, P.; Gurzov, E. N.; Chen, P.; Pilkington, E. H.; Stanley, W. J.; Litwak, S. A.; Davis, T. P.; Ke, P. C.; Ding, F. *Phys. Chem. Chem. Phys.* **2016**, 18, 94-100.
4. Wang, B.; Seabrook, S. A.; Nedumpully-Govindan, P.; Chen, P.; Yin, H.; Waddington, L.; Epa, V. C.; Winkler, D. A.; Kirby, J. K.; Ding, F. *Phys. Chem. Chem. Phys.* **2015**, 17, 1728-1739.
5. Shirvanyants, D.; Ding, F.; Tsao, D.; Ramachandran, S.; Dokholyan, N. V. *J. Phys. Chem. B* **2012**, 116, 8375-8382.
6. Lazaridis, T.; Karplus, M. *Curr. Opin. Struc. Biol.* **2000**, 10, 139-145.
7. Ding, F.; Borreguero, J. M.; Buldyrey, S. V.; Stanley, H. E.; Dokholyan, N. V. *Proteins: Structure, Function, and Bioinformatics* **2003**, 53, 220-228.
8. Debye, P.; Hückel, E. *Physikalische Zeitschrift* **1923**, 24, 185-206.
9. Akkermans, C.; Venema, P.; van der Goot, A. J.; Gruppen, H.; Bakx, E. J.; Boom, R. M.; van der Linden, E. *Biomacromolecules* **2008**, 9, 1474-1479.
10. Nelson, R.; Sawaya, M. R.; Balbirnie, M.; Madsen, A. Ø.; Riekel, C.; Grothe, R.; Eisenberg, D. *Nature* **2005**, 435, 773-778.
11. Marshall, K. E.; Serpell, L. C. *Soft Matter* **2010**, 6, 2110-2114.
12. Lu, K.; Jacob, J.; Thiyagarajan, P.; Conticello, V. P.; Lynn, D. G. *J. Am. Chem. Soc.* **2003**, 125, 6391-6393.
13. Rodriguez, J. A.; Ivanova, M. I.; Sawaya, M. R.; Cascio, D.; Reyes, F. E.; Shi, D.; Sangwan, S.; Guenther, E. L.; Johnson, L. M.; Zhang, M. *Nature* **2015**, 525, 486-490.
14. Krotee, P.; Rodriguez, J. A.; Sawaya, M. R.; Cascio, D.; Reyes, F. E.; Shi, D.; Hattne, J.; Nannenga, B. L.; Oskarsson, M. E.; Philipp, S. *eLife* **2017**, 6, e19273.
15. Hughes, Z. E.; Wright, L. B.; Walsh, T. R. *Langmuir* **2013**, 29, 13217-13229.

16. Loch, J.; Polit, A.; Górecki, A.; Bonarek, P.; Kurpiewska, K.; Dziedzicka- Wasylewska, M.; Lewiński, K. *J. Mol. Recognit.* **2011**, 24, 341-349.
17. Bolisetty, S.; Mezzenga, R. *Nat. Nanotech.* **2016**, 11, 365-371.
18. Goldschmidt, L.; Teng, P. K.; Riek, R.; Eisenberg, D. *Proc. Nat. Acad. Sci. USA* **2010**, 107, 3487-3492.
19. Luca, S.; Yau, W.-M.; Leapman, R.; Tycko, R. *Biochemistry* **2007**, 46, 13505-13522.